J. Fluid Mech. (2023), *vol*. 956, A9, doi:10.1017/jfm.2023.20

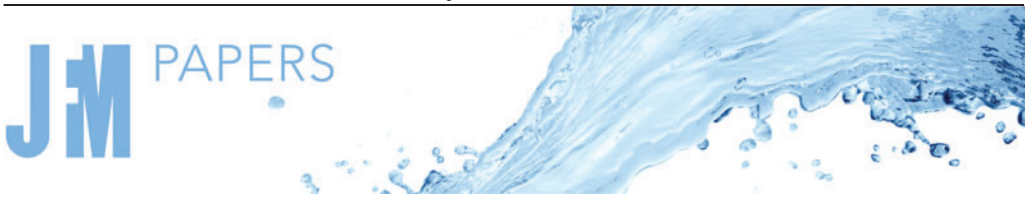

Predicting radial profiles for jets with arbitrary buoyancy

L. Milton-McGurk[1],†, N. Williamson[1] and S.W. Armfield[1]

[1]Department of Aerospace, Mechanical and Mechatronic Engineering, University of Sydney, NSW 2006, Australia

(Received 9 June 2022; revised 24 November 2022; accepted 3 January 2023)

The present study investigates the profiles of statistically axisymmetric turbulent jets with arbitrary buoyancy. Analytical expressions for the shape of the radial velocity, Reynolds stress and radial scalar flux profiles are derived from the governing equations by assuming self-similar Gaussian mean velocity and scalar profiles. Previously these have only been derived for the special cases of pure jets and plumes, whereas the present study generalises them to arbitrary buoyancies. These are then used to derive analytical expressions for the turbulent Schmidt/Prandtl numbers, which, along with the mean profiles, are shown to give predictions in agreement with existing literature.

Key words: plumes/thermals, buoyant jets, jets

1. Introduction

Axisymmetric jets and plumes occur when a turbulent flow exits a round source into a homogeneous (non-stratified) quiescent environment. If the density of the flow is equal to that of the ambient, then we refer to this as a neutral jet (J). If there is a density difference between the flow and ambient, then there will also be a buoyancy force, which, in the case of a vertically aligned source, may either be in the same or opposite direction to the axial momentum. When it is in the same direction as the flow, then we call this a positively buoyant jet (PBJ), whereas negatively buoyant jets (NBJs) occur when the buoyancy opposes the momentum. Both these flows can be characterised by their local Richardson number, Ri, the ratio of buoyancy to momentum, where $Ri > 0$ in PBJs and $Ri < 0$ in NBJs. Pure plumes are a similar axisymmetric free shear flow, but where Ri is constant and positive everywhere. In the far field, all PBJs approach this state (Fischer *et al.* 1979).

† Email address for correspondence: liam.milton-mcgurk@sydney.edu.au

Jets and PBJs have a similar 'jet-like' structure, where they expand as they entrain ambient fluid, have Gaussian mean velocity and scalar profiles, and eventually reach a state of self-similarity in the far field (Papanicolaou & List 1988; Panchapakesan & Lumley 1993; Wang & Law 2002; van Reeuwijk *et al.* 2016). NBJs, which have initially positive momentum but negative buoyancy, will rise if ejected vertically upwards with their momentum flux reducing with height due to their opposing buoyancy until the flow stagnates. After this, the flow reverses direction and collapses back onto itself, mixing with the opposing fluid and forming a fountain. The initial stage, before the return flow is formed, is what we refer to as an NBJ. This has a similar structure to jets/PBJs and also has Gaussian velocity/scalar profiles (Milton-McGurk *et al.* 2020, 2021, 2022; Talluru *et al.* 2021).

By invoking the conservation of mass and momentum, and assuming that the mean velocity and scalar (or buoyancy) profiles are self-similar and Gaussian, previous studies have derived analytical expressions for the mean radial velocity, $\bar{u}$, and Reynolds stress, $\overline{w'u'}$, profiles for the case of a neutral jet and plume (Mih 1989; Agrawal & Prasad 2003). This is possible by making use of the 'entrainment assumption', that the radial velocity of fluid entrained into the jet/plume is proportional to a characteristic velocity at that height by an entrainment coefficient, α (Morton, Taylor & Turner 1956). In pure jets and plumes, α is constant with values reported in the literature in the ranges $0.065 \lesssim \alpha_j \lesssim 0.080$ and $0.10 \lesssim \alpha_p \lesssim 0.16$, respectively (Fischer *et al.* 1979; Carazzo, Kaminski & Tait 2006). The derivations of these analytical profiles make use of the decay rate of the axial velocity scale and the radial expansion rate, which arise from the conservation equations under the assumption of self-similarity, and are simple power laws in the case of pure jets and plumes (Priestley & Ball 1955; Morton *et al.* 1956; Rajaratnam 1976; Fischer *et al.* 1979). For PBJs and NBJs, α is not constant and instead depends on the local Richardson number, Ri, and the velocity decay and expansion rates are not simple power laws (Morton 1959; Fox 1970; Kaminski, Tait & Carazzo 2005; van Reeuwijk & Craske 2015; Milton-McGurk *et al.* 2021, 2022). Owing to this, there has not yet been any attempt to derive analytical expressions for $\bar{u}$, $\overline{w'u'}$ or $\overline{u'b'}$ for jets with arbitrary buoyancy (e.g. PBJs or NBJs) based on the assumption of Gaussian axial velocity profiles. This is the purpose of the present study, which will use analytical expressions for α and the velocity decay/expansion rates to derive these expressions and compare them to measurements from our previous work (Milton-McGurk *et al.* 2021), as well as other experimental and numerical data in the literature (Wang & Law 2002; Darisse, Lemay & Benaïssa 2013; van Reeuwijk *et al.* 2016).

2. Governing equations

For a high-Reynolds-number, statistically axisymmetric flow in a homogeneous environment, and invoking the Boussinesq approximation, the conservation of volume, axial momentum, buoyancy and axial kinetic energy are

$$\frac{\partial}{\partial r}\left(r\bar{u}\right) + \frac{\partial}{\partial z}\left(r\bar{w}\right) = 0, \tag{2.1}$$

$$\frac{\partial}{\partial r}\left(r\bar{u}\bar{w} + r\overline{u'w'}\right) + \frac{\partial}{\partial z}\left(r\bar{w}^2\right) = r\bar{b}, \tag{2.2}$$

$$\frac{\partial}{\partial r}\left(r\bar{u}\bar{b} + r\overline{u'b'}\right) + \frac{\partial}{\partial z}\left(r\bar{w}\bar{b}\right) = 0, \tag{2.3}$$

$$\frac{\partial}{\partial r}\left(r\bar{u}\bar{w}^2 + 2r\overline{u'w'}\bar{w}\right) + \frac{\partial}{\partial z}\left(r\bar{w}^3\right) = 2r\overline{u'w'}\frac{\partial \bar{w}}{\partial r} + 2r\bar{w}\bar{b}, \tag{2.4}$$

where all pressure terms, and higher-order turbulence contributions involving $\overline{w'b'}$ and $\overline{w'^2}$, are neglected (Kaminski *et al.* 2005; van Reeuwijk & Craske 2015). Here $w = w(r, \phi, z)$ and $u = u(r, \phi, z)$ are the instantaneous axial and radial velocities corresponding to coordinates z and r, respectively, and $b = g\Delta\rho/\rho_a$ is the buoyancy. The azimuthal component, ϕ, disappears when averaging because the flow is assumed to be axisymmetric, and so we have $\bar{w} = \bar{w}(r, z)$, $\bar{b} = \bar{b}(r, z)$, etc. The gravitational acceleration is denoted by g and $\Delta\rho$ is the difference between the local and ambient density, ρ_a. For NBJs, $\Delta\rho < 0$, whereas $\Delta\rho > 0$ in PBJs and plumes. The buoyancy and scalar concentration are related by a constant such that $b = c\Delta\rho_o g/\rho_a$, where $\Delta\rho_o$ is the density difference between the plume/jet with the ambient at the source. All instantaneous quantities may be decomposed into their mean and fluctuating components, e.g. $w = \bar{w} + w'$.

The fluxes of volume, momentum, buoyancy and integral buoyancy, Q, M, F and B, may be defined from the mean velocity and buoyancy profiles,

$$Q = 2\int_0^\infty \bar{w} r \,\mathrm{d}r, \quad M = 2\int_0^\infty \bar{w}^2 r \,\mathrm{d}r, \quad F = 2\int_0^\infty \bar{w}\bar{b} r \,\mathrm{d}r, \quad B = 2\int_0^\infty \bar{b} r \,\mathrm{d}r, \tag{2.5a–d}$$

which have been scaled to remove a factor of π. These allow local velocity, length and buoyancy scales to be defined,

$$w_m = \frac{M}{Q}, \quad r_m = \frac{Q}{M^{1/2}}, \quad b_m = \frac{BM}{Q^2}, \tag{2.6a–c}$$

as well as the local Richardson number,

$$Ri = \frac{b_m r_m}{w_m^2}. \tag{2.7}$$

Equations (2.1)–(2.4) may then be integrated with respect to r from zero to infinity to obtain the following system of ordinary differential equations (ODEs),

$$\frac{\mathrm{d}Q}{\mathrm{d}z} = 2\alpha M^{1/2} \tag{2.8}$$

$$\frac{\mathrm{d}M}{\mathrm{d}z} = B = \frac{FQ}{\theta_m M} \tag{2.9}$$

$$\frac{\mathrm{d}F}{\mathrm{d}z} = 0 \tag{2.10}$$

$$\frac{\mathrm{d}}{\mathrm{d}z}\left(\gamma_m \frac{M^2}{Q}\right) = \delta_m \frac{M^{5/2}}{Q^2} + 2F, \tag{2.11}$$

where the entrainment coefficient, α, is defined as

$$(r\bar{u})_{r=\infty} = -\alpha r_m w_m. \tag{2.12}$$

The quantities θ_m, γ_m and δ_m are referred to as the 'profile coefficients', and can be interpreted as the dimensionless buoyancy flux, mean kinetic energy and turbulence

production,

$$\left.\begin{aligned}\theta_m &= \frac{F}{w_m b_m r_m^2},\\ \gamma_m &= \frac{2}{w_m^3 r_m^2}\int_0^\infty \bar{w}^3 r\,\mathrm{d}r,\\ \delta_m &= \frac{4}{w_m^3 r_m}\int_0^\infty \overline{w'u'}\frac{\partial \bar{w}}{\partial r} r\,\mathrm{d}r.\end{aligned}\right\} \tag{2.13}$$

By combining (2.8), (2.9) and (2.11), van Reeuwijk & Craske (2015) derived the following expression for α, which makes no assumptions about the shape of the profiles but assumes they are self-similar,

$$\alpha = -\frac{\delta_m}{2\gamma_m} + \left(1 - \frac{\theta_m}{\gamma_m}\right) Ri \tag{2.14}$$

as well as the following equation for the spreading rate,

$$\frac{\mathrm{d}r_m}{\mathrm{d}z} = -\frac{\delta_m}{\gamma_m} + \frac{3}{2}\left(1 - \frac{4}{3}\frac{\theta_m}{\gamma_m}\right) Ri. \tag{2.15}$$

Using a similar approach, the following expressions describing the development of the velocity and buoyancy scales may also be derived:

$$\frac{r_m}{w_m}\frac{\mathrm{d}w_m}{\mathrm{d}z} = \frac{\delta_m}{\gamma_m} + \left(\frac{2\theta_m}{\gamma_m} - 1\right) Ri, \tag{2.16}$$

$$\frac{r_m}{b_m}\frac{\mathrm{d}b_m}{\mathrm{d}z} = \frac{\delta_m}{\gamma_m} - 2\left(1 - \frac{\theta_m}{\gamma_m}\right) Ri = -2\alpha. \tag{2.17}$$

By invoking the assumption of self-similar Gaussian mean velocity and buoyancy profiles, several additional simplifications can be made. For instance, let the velocity and buoyancy profiles be described by the shape functions f and y, respectively,

$$\bar{w}(r, z) = 2w_m f(\eta), \tag{2.18}$$

$$\bar{b}(r, z) = \frac{2b_m}{\lambda^2} y(\eta), \tag{2.19}$$

where $\eta = \sqrt{2}r/r_m$ and λ is the ratio of $1/e$ widths of the buoyancy and velocity profiles, r_b and r_w,

$$\lambda = \frac{r_b}{r_w}. \tag{2.20}$$

We then set

$$f(\eta) = \mathrm{e}^{-\eta^2}, \tag{2.21}$$

$$y(\eta) = \exp(-\eta^2/\lambda^2), \tag{2.22}$$

which is equivalent to assuming Gaussian mean velocity and buoyancy profiles that have centreline values $\bar{w}_c = 2w_m$ and $\bar{b}_c = 2b_m/\lambda^2$, and $1/e$ widths $r_w = r_m/\sqrt{2}$ and

$r_b = \lambda r_m/\sqrt{2}$. By evaluating the definitions of the profile coefficients in (2.13), we then have

$$\theta_m = \frac{2}{\lambda^2 + 1}, \quad \gamma_m = \frac{4}{3}. \tag{2.23a,b}$$

The entrainment coefficient, α in (2.14), therefore depends only on δ_m, λ and Ri.

For fully self-similar flows, such as pure jets ($Ri = 0$) and plumes ($Ri =$ constant) in the far field, all profile coefficients are constant. This assumption of self-similarity, along with the conservation equations (2.1)–(2.4) (or a simple dimensional analysis), leads to $w_m \sim z^{-1}$ and $w_m \sim z^{-1/3}$ in pure jets and plumes, respectively, and $r_m \sim z$ in both (Priestley & Ball 1955; Morton *et al.* 1956; Rajaratnam 1976; Fischer *et al.* 1979). Previous studies have used these results to derive analytical expressions for $\bar{u}$, $\overline{w'u'}$ and $\overline{u'b'}$ for these limiting cases by assuming Gaussian mean profiles (Mih 1989; Agrawal & Prasad 2003). The following sections will instead use (2.14)–(2.17) to derive expressions for these profiles in terms of the profile coefficients in (2.13). Although these assumptions are more questionable in PBJs and NBJs, we argue that, provided appropriate values of λ and δ_m are used for a given Ri, they are still reasonable approximations and lead to predictions consistent with existing experimental and numerical data. The expressions will therefore be applicable to turbulent jets with arbitrary buoyancy, rather than only the limiting cases of pure jets and plumes.

3. Analytical expressions for profiles

3.1. *Radial velocity*

Let the mean radial velocity profile be described by shape function, $h(\eta)$, such that

$$\bar{u}(r, z) = 2w_m h(\eta). \tag{3.1}$$

By inserting this into the continuity equation (2.1), and using (2.18) and (2.21), the following expression for the shape of the radial velocity profile may be derived:

$$h = \frac{\sqrt{2}}{2\eta}\left(\mathrm{e}^{-\eta^2}\left(\eta^2 \frac{\mathrm{d}r_m}{\mathrm{d}z} + \alpha\right) - \alpha\right). \tag{3.2}$$

By substituting the equations for $\mathrm{d}r_m/\mathrm{d}z$ and α into (2.15) and (2.14), the following is obtained:

$$h = \frac{\sqrt{2}}{2\eta}\left(\mathrm{e}^{-\eta^2}\left[-\frac{3}{4}\delta_m\left(\eta^2 + \frac{1}{2}\right) + \left(\frac{3}{2}(1 - \theta_m)\,\eta^2 + 1 - \frac{3}{4}\theta_m\right) Ri\right] - \alpha\right). \tag{3.3}$$

Provided $\bar{w}$ can be described by a Gaussian profile, this is valid for self-similar axisymmetric turbulent jets with arbitrary buoyancy, and is consistent with previously derived expressions for the limiting cases of pure jets/plumes (Mih 1989; Agrawal & Prasad 2003). By using the expression for α in (2.14), and observing (2.23*a*,*b*), this equation for h depends only on λ, δ_m and Ri.

3.2. *Reynolds stress*

Let the self-similar Reynolds stress profile be written in terms of shape function $j(\eta)$,

$$\overline{w'u'}(r, z) = 4w_m^2 j(\eta). \tag{3.4}$$

This can be substituted for $\overline{w'u'}$ in the momentum equation, (2.2), along with shape functions (2.18), (2.19) and (3.1) for $\bar{w}$, $\bar{b}$ and $\bar{u}$, to derive

$$\frac{\partial}{\partial \eta}(\eta j) = \sqrt{2}\eta^2 f \frac{\mathrm{d}r_m}{\mathrm{d}z}\frac{\partial f}{\partial \eta} - \sqrt{2}\eta f^2 \frac{r_m}{w_m}\frac{\mathrm{d}w_m}{\mathrm{d}z} - \frac{\partial}{\partial \eta}(\eta f h)\frac{Ri\sqrt{2}}{4\lambda^2} y\eta, \tag{3.5}$$

after performing a change of variables to express the partial derivatives in terms of η instead of r and z. By substituting the Gaussian functions in (2.21) and (2.22) for f and y, this may be integrated with respect to η to give

$$\begin{aligned} j = \frac{\sqrt{2}}{4\eta}\Bigg(&\frac{\mathrm{d}r_m}{\mathrm{d}z}\left[\exp(-2\eta^2)(2\eta^2+1)-1\right] + \frac{r_m}{w_m}\frac{\mathrm{d}w_m}{\mathrm{d}z}\left(\exp(-2\eta^2)-1\right) \\ &+\frac{Ri}{2}\left(1-\exp(-\eta^2/\lambda^2)\right)\Bigg) - \mathrm{e}^{-\eta^2}h, \end{aligned} \tag{3.6}$$

where the constant of integration is obtained by considering the limit as $\eta \to 0$ and assuming that $\overline{w'u'}$ is bounded at $\eta = 0$ (Agrawal & Prasad 2003). The following may then by obtained by inserting (2.15) and (2.16), and using the derived expression for h,

$$j = \frac{\sqrt{2}}{2\eta}\left(\alpha\,\mathrm{e}^{-\eta^2} - \exp(-2\eta^2)\left[-\frac{3}{8}\delta_m + \frac{3}{4}(1-\theta_m)\,Ri\right] - \frac{Ri}{4}\exp(-\eta^2/\lambda^2)\right). \tag{3.7}$$

3.3. *Radial scalar flux*

Now consider the shape function, p, corresponding to the radial scalar flux profile,

$$\overline{u'b'} = \frac{4w_m b_m}{\lambda^2} p(\eta). \tag{3.8}$$

By inserting (3.8) into the conservation of buoyancy equation (2.3), and using the expression for h in (3.2) and $\mathrm{d}b_m/\mathrm{d}z$ in (2.17), the following may be derived:

$$p = \frac{\sqrt{2}}{2\eta}\alpha\exp(-\eta^2/\lambda^2)\left(1-\mathrm{e}^{-\eta^2}\right). \tag{3.9}$$

4. Comparisons with experimental data

The shape functions, h, j and p derived in § 3 for the radial velocity, Reynolds stress and radial scalar flux profiles depend only on λ, δ_m and Ri. The width ratio, λ, is typically found to be constant in pure jets and plumes in the far field, with values of $\lambda_j \simeq 1.2$ and $\lambda_p \simeq 1.0$, respectively (Papanicolaou & List 1988; Shabbir & George 1994; Wang & Law 2002; Ezzamel, Salizzoni & Hunt 2015; van Reeuwijk *et al.* 2016). The value in real PBJs may vary somewhat as they develop, but approach approximately $\lambda = 1.0$ in the far field as the flow approaches a pure plume-like state where $Ri \to Ri_p$ (Panchapakesan & Lumley 1993; Wang & Law 2002; Ezzamel *et al.* 2015; van Reeuwijk *et al.* 2016). In Gaussian PBJs/plumes, it was shown in Milton-McGurk *et al.* (2022) that a value of $\lambda = 1$ or $1/\sqrt{2}$

is required to maintain consistency between the conservation of mass, momentum, kinetic energy, and an additionally derived $\bar{w}^3$ equation. As a value of $\lambda = 1$ is consistent with both existing literature and the conservation equations, this will be used in the present study when considering PBJs and plumes. In NBJs, which do not approach a constant Ri value, λ is not constant and has been shown to increase between $1.3 \lesssim \lambda \lesssim 1.5$ over $-0.03 \gtrsim Ri \gtrsim -0.3$ (Milton-McGurk *et al.* 2021). However, reasonable velocity predictions were obtained in Milton-McGurk *et al.* (2021) by assuming a constant $\lambda \simeq 1.46$, and solving an integral model of the flow.

The dimensionless turbulence production, δ_m, has been found to be approximately constant in pure jets and plumes, and although there is some variation in the literature ($-0.23 \lesssim \delta_m \lesssim -0.20$ in plumes, $-0.21 \lesssim \delta_m \lesssim -0.19$ in jets), $\delta_m \simeq -0.20$ in both cases (Wang & Law 2002; Ezzamel *et al.* 2015; van Reeuwijk & Craske 2015; van Reeuwijk *et al.* 2016). van Reeuwijk *et al.* (2016) also reported an approximately constant value in PBJs, although this was slightly lower in magnitude than the jet and plume values with $\delta_m \simeq -0.175$. In NBJs, δ_m is not constant and was found in Milton-McGurk *et al.* (2021) to become increasingly negative as $Ri \to -\infty$, approximately following the linear relation,

$$\delta_m = \delta_j + \tilde{\delta} Ri. \tag{4.1}$$

Here $\delta_j \simeq -0.2$ is the 'neutral jet value', and $\tilde{\delta} \simeq 0.604$ is an *ad hoc* empirical term that captures the observed variation of δ_m with Ri.

For the remainder of this section, we use these aforementioned values of δ_m and λ as inputs into shape functions h, j and h for a given Ri. Although these are only approximations for the intermediate cases of PBJs and NBJs, we see that they lead to good agreement with existing data. In the case of pure jets and plumes, we have that $Ri_j = 0$ and $Ri_p = 8\alpha_p/5$, respectively (van Reeuwijk & Craske 2015). For Gaussian velocity/scalar profiles and $\lambda_p = 1.0$, this leads to $\alpha_j = -3\delta_m/8$ and $\alpha_p = -5\delta_m/8$ using (2.14). Substituting these values into (3.3) and (3.7) gives equivalent expressions to those derived by Agrawal & Prasad (2003) and Mih (1989). These were found to be in reasonable agreement with existing experimental data and so are not explored further here. However, the application of h, j and p to PBJs and NBJs, and p to pure jets, has not been considered until now.

Figure 1 shows normalised $\overline{u'c'}$ profiles for a pure jet and plume obtained from an experimental study by the previous authors (Milton-McGurk *et al.* 2021) (jet only), as well as direct numerical simulation (DNS) data from van Reeuwijk *et al.* (2016), and the best fit profiles of experiments by Wang & Law (2002). The predictions corresponding to p for both flows is also shown, where $\delta_m = -0.20$ and $\lambda = 1.2$ for the jet, and $\delta_m = -0.20$ and $\lambda = 1.0$ for the plume. Although there is some small variation between data from the three studies, they are all in reasonable agreement with each other and p for both the jet and plume cases.

Figure 2 shows normalised $\bar{u}$, $\overline{w'u'}$ and $\overline{u'b'}$ profiles for a PBJ from van Reeuwijk *et al.* (2016). Also shown are the corresponding h, j and p profiles with $\delta_m = -0.175$ and $\lambda = 1.0$. The local Ri corresponding to the profiles from van Reeuwijk *et al.* (2016), and hence used for h, j and p, were estimated as $Ri \simeq 0.042$ and 0.084. Only one Ri profile is shown for $\overline{w'u'}$, because for the case where $\lambda = 1$, (3.7) for j simplifies to a form that is not dependent on Ri. There is good agreement between the analytical profiles and those from van Reeuwijk *et al.* (2016) for $\bar{u}$, $\overline{w'u'}$ and $\overline{u'b'}$ at both Ri locations. Also shown are the predictions for pure jets and plumes, so that we may observe whether there is any improvement gained by using the presently derived expressions for arbitrary Ri. Here we set $\lambda = 1$ for both cases, because this is more appropriate for PBJs than the usual $\lambda = 1.2$

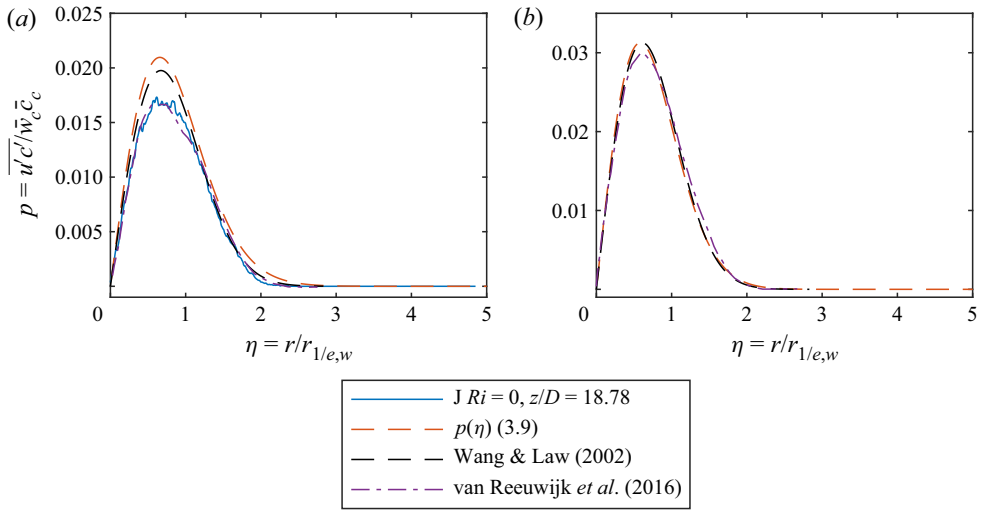

Figure 1. The shape function p, defined in (3.9), for the case of a neutral jet ($\lambda = 1.2$, $\delta_m = -0.20$) in (a), and pure plume ($\lambda = 1.0$, $\delta_m = -0.20$) in (b). The corresponding normalised radial scalar flux profiles obtained in an experimental study by the present authors (jet only) (Milton-McGurk *et al.* 2020, 2021), as well as by Wang & Law (2002) and van Reeuwijk *et al.* (2016), are also shown.

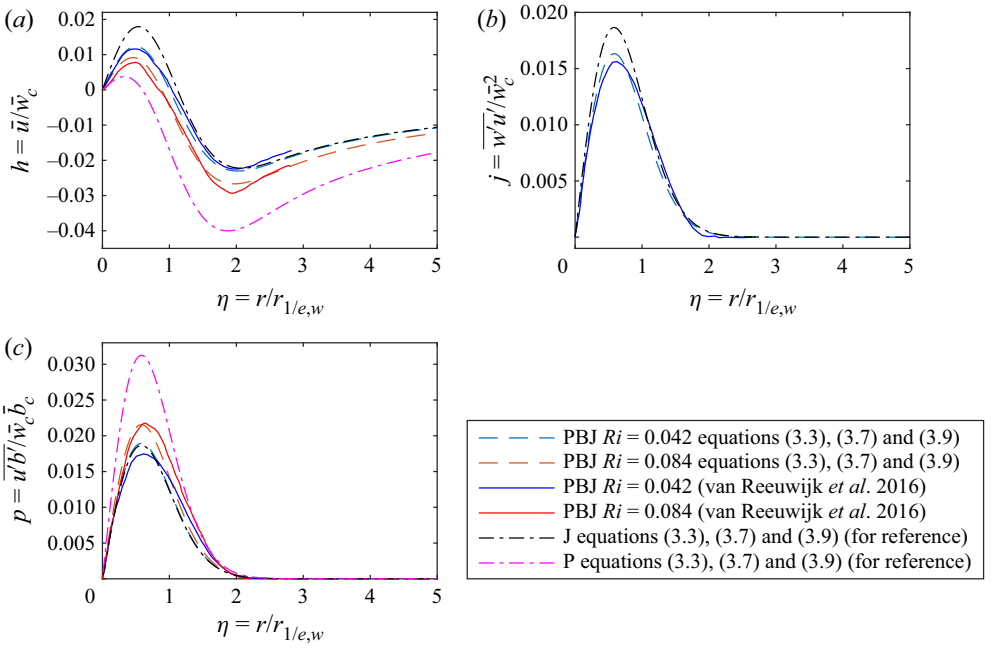

Figure 2. The shape functions h, j and p defined in (3.3), (3.7) and (3.9), respectively, are shown in (a)–(c) for the case of a PBJ with $\lambda = 1.0$ and $\delta_m = -0.175$ at $Ri = 0.042$ and $Ri = 0.084$. The corresponding normalised radial velocity, Reynolds stress and radial scalar flux profiles obtained from DNS study by van Reeuwijk *et al.* (2016) are also shown in each case. The analytical expressions for a pure jet (J) and plume (P) are also shown as a reference.

value for pure jets (Milton-McGurk *et al.* 2022). The p prediction for a J is very close to that for the $Ri = -0.042$ PBJ in figure 2(c), because, in this case, the only difference between predictions is due to α. For $Ri = -0.042$, the flow is still quite 'jet-like' and so

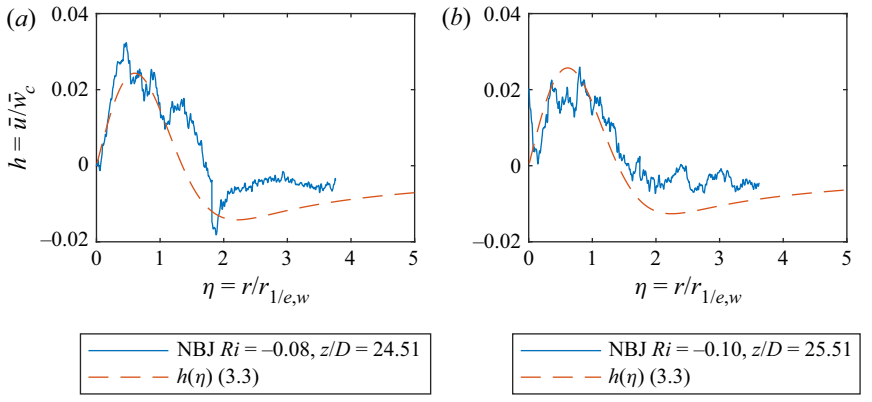

Figure 3. The shape function h, defined in (3.3), for the case of an NBJ with $\lambda = 1.46$ and $\delta_m \sim Ri$ (as defined by (4.1)) at $Ri = -0.08$ in (a) and $Ri = -0.10$ in (b). The corresponding normalised radial velocity profiles obtained in an experimental study by the present authors are also shown (Milton-McGurk *et al.* 2020, 2021).

these values are similar for a PBJ ($\alpha = 0.076$) and J ($\alpha = 0.075$). For $Ri = -0.084$, the arbitrary-Ri relation has considerably better agreement for p, which is also the case at both Ri in figure 2(a) for h. As the Reynolds stress profile, j, is independent of Ri when $\lambda = 1$, the function is the same for pure jets/plumes/PBJs with this λ, and is therefore controlled by δ_m. This value is approximately the same for jets/plumes ($\delta_m \simeq -0.20$), and is slightly lower for PBJs ($\delta_m \simeq -0.175$) (van Reeuwijk *et al.* 2016). The J prediction shown in figure 2(c) corresponds to $\delta_m = -0.20$, which does not have as good agreement as the PBJ prediction using $\delta_m = -0.175$.

Figures 3–5 show normalised $\bar{u}$, $\overline{w'u'}$ and $\overline{u'b'}$ profiles for an NBJ at two Ri locations. These experimental data were gathered in previous studies by the present authors using combined particle image velocimetry (PIV) and planar laser-induced fluorescence (PLIF), with additional details available in Milton-McGurk *et al.* (2020) and Milton-McGurk *et al.* (2021). The corresponding analytical h, j and p expressions are also shown, obtained by assuming a constant $\lambda = 1.46$ and the linear expression for δ_m in (4.1), along with the Ri value corresponding to the experimental data. Reasonable agreement is found for h in figure 3, whereas j and p in figures 4 and 5 show excellent agreement.

At the top of an NBJ, $w_m \to 0$ and $Ri \to -\infty$ as the mean flow velocity stagnates. After this, the flow reverses direction and eventually forms a fully developed fountain. The region where the fluid reverses direction is referred to as the 'cap' region, which occurs in the model by Hunt & Debugne (2016) of a fully developed fountain at $Ri = -0.5$. The present analysis and hence the h, j and p expressions are unlikely to be valid in NBJs near this region, where the flow is no longer jet-like (Milton-McGurk *et al.* 2021; Talluru, Williamson & Armfield 2022). The agreement between the profile predictions and NBJ data in figures 3–5 suggest that the locations with $Ri = -0.08$ and -0.10 are sufficiently far from the cap region that the present assumptions remain reasonable. However, in the NBJ data (Milton-McGurk *et al.* 2021), the profiles began to depart from the predictions for $Ri \lesssim -0.11$, and so the expressions may longer be valid in this region.

5. Turbulent Prandtl/Schmidt number

The derived expressions for Reynolds stress and radial scalar flux may also be used to obtain an expression for the turbulent Schmidt number, Sc_T,

$$Sc_T = \frac{\nu_T}{\kappa_T}, \tag{5.1}$$

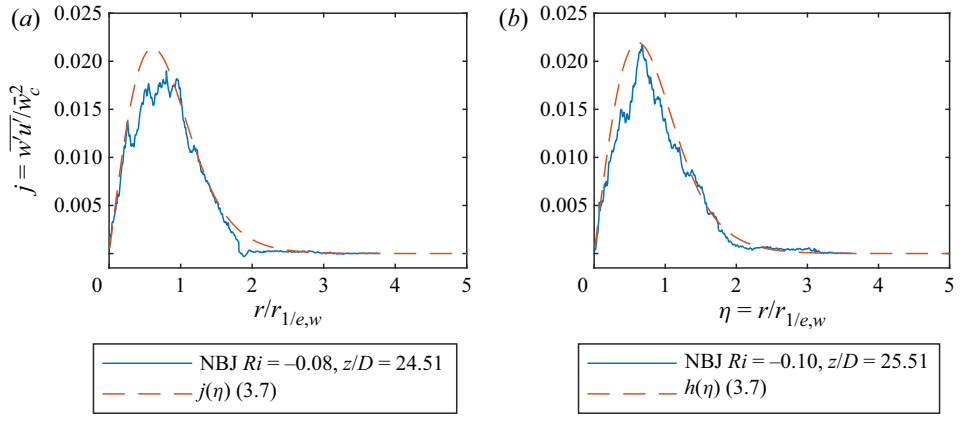

Figure 4. The shape function j, defined in (3.7), for the case of an NBJ with $\lambda = 1.46$ and $\delta_m \sim Ri$ (as defined by (4.1)) at $Ri = -0.08$ in (*a*) and $Ri = -0.10$ in (*b*). The corresponding normalised Reynolds stress profiles obtained in an experimental study by the present authors are also shown (Milton-McGurk *et al.* 2020, 2021).

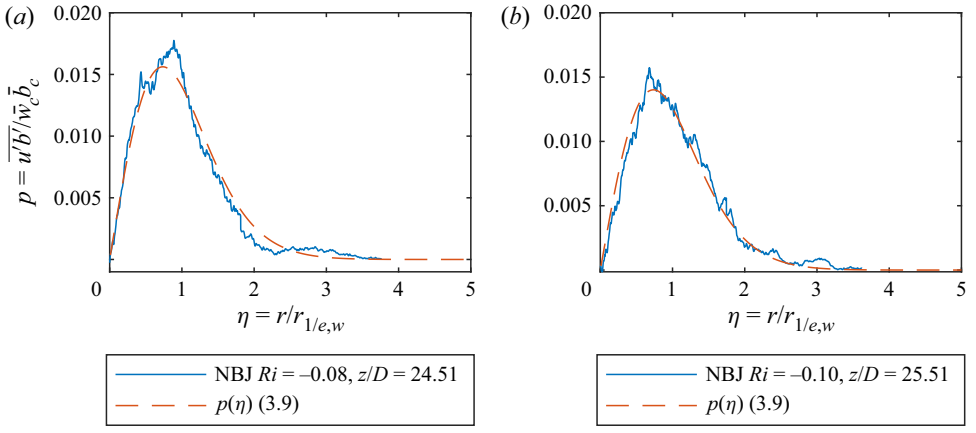

Figure 5. The shape function p, defined in (3.9), for the case of an NBJ with $\lambda = 1.46$ and $\delta_m \sim Ri$ (as defined by (4.1)) at $Ri = -0.08$ in (*a*) and $Ri = -0.10$ in (*b*). The corresponding normalised radial scalar flux profiles obtained in an experimental study by the present authors are also shown (Milton-McGurk *et al.* 2020, 2021).

where ν_T and κ_T are the momentum and mass diffusivities, respectively,

$$\nu_T = -\frac{\overline{w'u'}}{\partial\bar{w}/\partial r}, \quad \kappa_T = -\frac{\overline{u'b'}}{\partial\bar{b}/\partial r}. \tag{5.2a,b}$$

As the experiments reported in Milton-McGurk *et al.* (2020, 2021) used saline as the scalar tracer, we use the turbulent Schmidt number here rather than the turbulent Prandtl number, Pr_T. The same expressions also apply to Pr_T, except κ_T would instead refer to thermal diffusivity. By using (3.7) and (3.9) for j and p, along with the Gaussian functions in (2.21) and (2.19) for f and y, the following analytical expressions for 'non-dimensional'

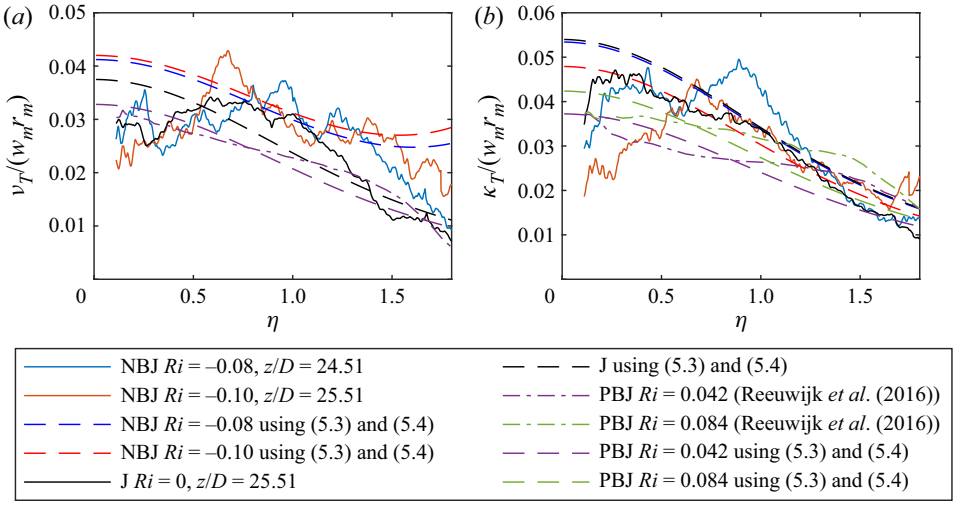

Figure 6. Non-dimensional turbulent momentum, ν_T, and mass, κ_T, diffusivity calculated from the NBJ and J data obtained in Milton-McGurk *et al.* (2020, 2021) and PBJ data in van Reeuwijk *et al.* (2016). The analytical expressions given in (5.3)–(5.4) are also shown.

ν_T and κ_T may be derived,

$$\frac{\nu_T}{w_m r_m} = \frac{1}{2\eta^2}\left(\alpha - \mathrm{e}^{-\eta^2}\left(-\frac{3}{8}\delta_m + \frac{3}{4}\left(1-\theta_m\right)Ri\right) - \frac{Ri}{4}\exp\left(\eta^2\left(1-1/\lambda^2\right)\right)\right), \tag{5.3}$$

$$\frac{\kappa_T}{w_m r_m} = \frac{1}{2\eta^2}\alpha\lambda^2\left(1-\mathrm{e}^{-\eta^2}\right). \tag{5.4}$$

These analytical profiles are shown alongside experimental data from Milton-McGurk *et al.* (2020, 2021) in figure 6 for an NBJ at two local Ri and a neutral jet ($Ri = 0$, $\lambda = 1.2$). To the best of the authors' knowledge, this is the first time turbulent momentum and mass/thermal diffusivity data have been presented for an NBJ. Profiles for a PBJ, obtained using data in van Reeuwijk *et al.* (2016), is also shown alongside their corresponding predictions. For $\kappa_T/(w_m r_m)$, PBJ data and predictions at two Ri are shown, whereas only one Ri is shown for $\nu_T/(w_m r_m)$ because this does not depend on Ri when $\lambda = 1$. The data are shown for $0.1 \lesssim \eta \lesssim 2$, because below this range the denominator of (5.2*a*,*b*) approaches zero, and above it both the numerator and denominator approach zero, resulting in growing numerical errors when computing ν_T and κ_T from the experimental data. For both NBJ cases, the J and the PBJ, the analytical expressions match the experimental data reasonably well for both $\nu_T/(w_m r_m)$ and $\kappa_T/(w_m r_m)$. For the NBJ, the data are reasonably similar for both Ri, which is also reflected in the analytical curves being reasonably close. These are also similar to the J case, where the analytical J prediction for $\kappa_T/(w_m r_m)$ almost matches that for the lower magnitude Ri (and, thus, more 'jet-like') NBJ.

By dividing (5.3) by (5.4), we arrive at the following expression for the turbulent Schmidt number:

$$Sc_T = \frac{\alpha - \mathrm{e}^{-\eta^2}\left(-\frac{3}{8}\delta_m + \frac{3}{4}\left(1-\theta_m\right)Ri\right) - \frac{Ri}{4}\exp\left(\eta^2\left(1-1/\lambda^2\right)\right)}{\alpha\lambda^2\left(1-\mathrm{e}^{-\eta^2}\right)}. \tag{5.5}$$

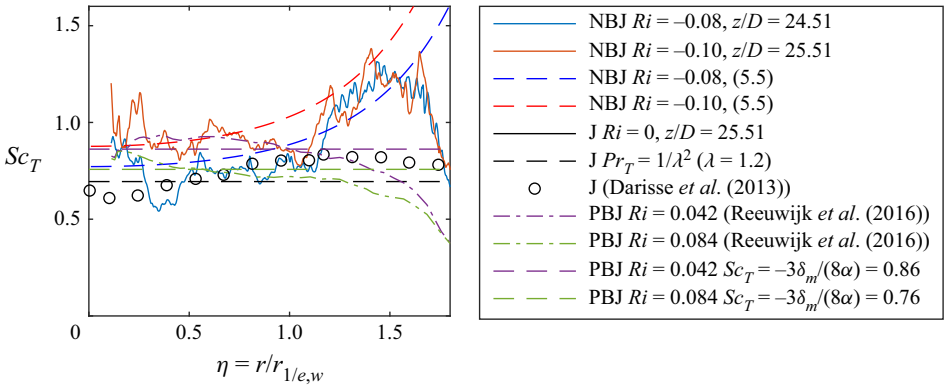

Figure 7. The turbulent Schmidt number, Sc_T, calculated from the NBJ and J data obtained in Milton-McGurk *et al.* (2020, 2021) and PBJ data in van Reeuwijk *et al.* (2016). The analytical expressions, as implied by (5.5), are also shown.

For a Gaussian pure jet with $Ri = 0$, we have from (2.14) that $\alpha_j = -3\delta_m/8$. When inserting these into (5.5), all dependence on η cancels out and we are left with a constant $Sc_T = 1/\lambda^2$. This result was also reported in Chen & Rodi (1980), and a similar result where $Sc_T \propto 1/\lambda^2$ in Craske, Salizzoni & van Reeuwijk (2017). The latter study derived it based on an alternative formulation for an 'integral turbulent Prandtl/Schmidt number', Pr_{Tm} and Sc_{Tm}, which were defined using several integral quantities, including characteristic scales for ν_T and κ_T that did not vary with radial distance. For Gaussian pure plumes with $\lambda = 1$, we have $Ri_p = 8\alpha_p/5$ and $\alpha_p = -5\delta_m/8$, which, when inserted into (5.5), also results in the η dependence cancelling out, leaving $Sc_T = 3/5$. This plume value is identical to that reported in Craske *et al.* (2017) for their Pr_{Tm}, and also agrees with DNS data from van Reeuwijk *et al.* (2016) ($Pr_{Tm} = 0.66$) and experimental data from Wang & Law (2002) ($Pr_{Tm} = 0.62$), as estimated by Craske *et al.* (2017). The present analysis supports this result, and additionally shows that, under the current assumptions, the standard definitions of Sc_T (and Pr_T) result in constant values across the width of both neutral jets and pure plumes, despite ν_T and κ_T being functions of radial distance. This is also the case for PBJs with $\lambda = 1$, where (5.5) gives a constant $Sc_T = -3\delta_m/(8\alpha)$ for a given Ri. When a radial dependence is observed in a real jet/PBJ/plume, it may, for instance, be due to a departure from idealised Gaussian shapes for the mean velocity/scalar profiles or, for PBJs/plumes, a non-unity width ratio between these profiles ($\lambda \neq 1$).

Experimental data from Milton-McGurk *et al.* (2020, 2021) are used to calculate Sc_T in a J and NBJ and DNS data in van Reeuwijk *et al.* (2016) for a PBJ. These are presented in figure 7 alongside the predictions of (5.5) and experimental J data by Darisse *et al.* (2013). The J data agree very well between Milton-McGurk *et al.* (2020, 2021) and Darisse *et al.* (2013), and are close to the prediction of $1/\lambda^2 = 0.694$ for $\lambda = 1.2$. For the PBJs, the inner Sc_T profiles are similar to the constant values predicted by (5.5) of $Sc_T = -3\delta_m/(8\alpha) \simeq 0.86$ and 0.76 for $Ri = 0.042$ and 0.084, respectively. The NBJ data also agree with the analytical expressions from (5.5), with both having similar shapes and lower magnitude for the smaller $-Ri$. The prediction for the NBJ, however, approaches infinity as $\eta \to \infty$, which reveals a limitation of the expression for larger η. In real NBJs, the mean velocity/scalar profiles are not exactly Gaussian, and will eventually decrease to zero at some finite η (unlike true Gaussian's which only approach zero at the limit). The same applies to neutral buoyant jets/PBJs and plumes under the present assumptions,

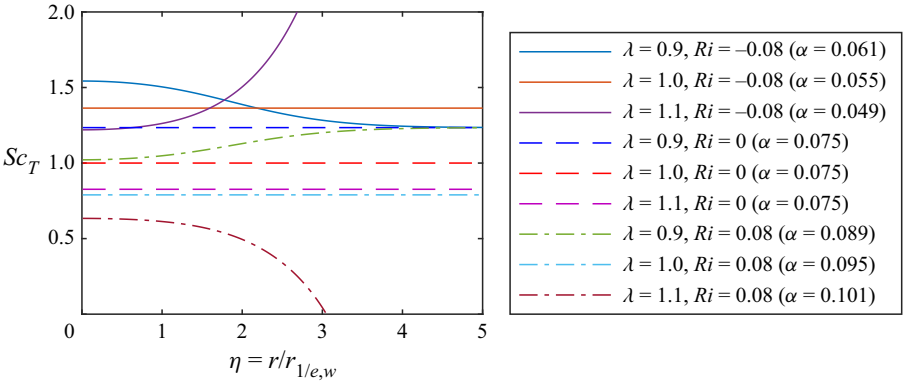

Figure 8. The turbulent Schmidt number, Sc_T, computed using (5.5), for several values of Ri and λ and a fixed $\delta_m = -0.2$. The corresponding value of α implied by (2.14) is also shown.

which, whereas (5.5) predicts they are constant for all η, in practice Sc_T will decrease to zero at the true 'edge' of the jet.

The value of λ in a given jet-like flow reflects the ratio of widths between the buoyancy and velocity profiles. An expression for spreading rate of the velocity profile, $\mathrm{d}r_m/\mathrm{d}z$, was given in (2.15), and depends on the profile coefficients and local Ri. It is also possible to derive an analogous expression for the buoyancy spreading rate, $\mathrm{d}r_{mb}/\mathrm{d}z$, where $r_{mb} = \sqrt{2}r_b = \lambda r_m$ for Gaussian profiles. This was done in Milton-McGurk *et al.* (2021) using (2.3) and an additional equation for 'mean squared buoyancy' (Craske *et al.* 2017). These spreading rates will determine the behaviour of λ, and are consequences of the conservation equations and values of the relevant profile coefficients. This, along with the local Ri, are what primarily influence the difference between the Sc_T presented in figure 7 in PBJs and NBJs. This is illustrated in figure 8, which shows the predictions of (5.5) for three choices of λ at three different Ri and a constant $\delta_m = -0.2$. Note that although, in NBJs, $\alpha < 0$ for sufficiently negative Ri (e.g. near the top), here we are only considering smaller magnitude Ri where the flow is more jet-like and $\alpha > 0$ (Milton-McGurk *et al.* 2021). For both NBJs and PBJs with $\lambda > 1$, where $Ri < 0$ and $Ri > 0$, we see that (5.5) diverges towards positive and negative infinity, respectively. For $\lambda < 1$, we have that $Sc_T \to 1/\lambda^2$, and for $\lambda = 1$, that $Sc_T = -3\delta_m/(8\alpha)$, for both PBJs and NBJs. When $Ri = 0$, i.e. neutral jets, we have a constant Sc_T regardless of λ. The present study has used $\lambda > 1$ for NBJs, and $\lambda = 1$ for PBJs, because this is consistent with the data and analysis in Milton-McGurk *et al.* (2022) and van Reeuwijk *et al.* (2016). However, $\lambda > 1$ is sometimes observed in PBJs (Wang & Law 2002; Ezzamel *et al.* 2015), which would lead to a diverging Sc_T prediction that is not physically realistic. The application of (5.5) should therefore be restricted to small values of η, where the assumption of Gaussian profiles is more reasonable than at the tails.

It is also useful to consider the limit of Sc_T as $\eta \to 0$, which, after applying L'Hôpitals's rule, can be expressed as

$$Sc_T\,(\eta = 0) = \frac{1}{4\alpha\lambda^2}\left(-\frac{3}{2}\delta_m + Ri\left[\frac{(\lambda^2-1)(2\lambda^2-1)}{\lambda^2(\lambda^2+1)}\right]\right), \tag{5.6}$$

which is plotted in figure 9 against Ri for $\delta_m = -0.2$ and three values of λ. In addition, table 1 gives a summary of the Sc_T predictions implied by (5.5)–(5.6) for the different Ri and λ cases. Although the $\eta \to \infty$ limits reflect the behaviour of the outer Sc_T profiles,

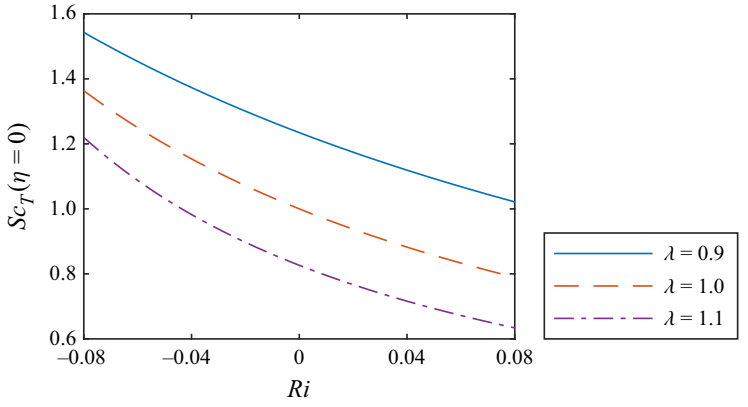

Figure 9. The $\eta \to 0$ limit of the turbulent Schmidt number, Sc_T, evaluated using (5.5), against local Ri for $\lambda = 0.9$, 1.0 and 1.1 and a fixed $\delta_m = -0.2$.

Ri	λ	Sc_T	$Sc_T(\eta = 0)$	$Sc_T(\eta \to \infty)$
<0	<1	(5.5)	(5.6)	$1/\lambda^2$
	1	$-3\delta_m/(8\alpha)$	$-3\delta_m/(8\alpha)$	$-3\delta_m/(8\alpha)$
	>1	(5.5)	(5.6)	∞
$=0$	<1	$1/\lambda^2$	$1/\lambda^2$	$1/\lambda^2$
	1	1	1	1
	>1	$1/\lambda^2$	$1/\lambda^2$	$1/\lambda^2$
>0	<1	(5.5)	(5.6)	$1/\lambda^2$
	1	$-3\delta_m/(8\alpha)$	$-3\delta_m/(8\alpha)$	$-3\delta_m/(8\alpha)$
	>1	(5.5)	(5.6)	$-\infty$

Table 1. Summary of the Sc_T predictions from (5.5) and (5.6), including the $\eta \to 0$ and $\eta \to \infty$ limits for different Ri and λ cases when $\alpha > 0$.

(5.6) characterises the magnitude for lower η where the predictions are more physically realistic. This expression, together with figure 8, therefore illustrates the sensitivity of Sc_T to both λ and Ri, and how they can contribute to producing the differences observed between PBJs and NBJs in figure 7. For instance, decreasing Ri increases $Sc_T(\eta = 0)$ for all λ shown in figure 9, which is also evident when observing the inner profile for all Ri cases shown in figure 8. In an NBJ, this implies that negative buoyancy increases Sc_T, acting to decrease thermal/mass diffusion relative to momentum diffusion. The opposite applies for increasingly buoyant PBJs. The value of δ_m also has an influence on Sc_T, although this is much less significant than λ and Ri, and so was kept constant in figures 8–9. Conversely, the profiles, h, j and p, are not very sensitive to λ, with their magnitude mostly controlled by δ_m and Ri. This can be observed in figure 2, where the pure jet and plume predictions ($Ri = 0$ versus $Ri_p \simeq 0.2$) are significantly different for h and p. For j, there is no Ri dependence when $\lambda = 1$ and the profiles magnitude is linearly proportional to δ_m, which gives rise to the the modest difference between the PBJ and jet predictions in figure 2(c).

Equations (5.3)–(5.1) for ν_T, κ_T and Sc_T all agree with the experimental data for the PBJ, NBJ and J for $\eta \lesssim 2$. The analytical pure plume result of $Sc_T = 3/5$ is also in

agreement with existing literature (Wang & Law 2002; van Reeuwijk *et al.* 2016; Craske *et al.* 2017). The present analysis has shown that the common assumptions of Gaussian mean velocity/scalar profiles can also be applied to NBJs and, given appropriate values of δ_m and λ are used, yield results consistent with experiments. This supports the idea that the processes behind turbulent momentum and mass/thermal diffusion are similar in NBJs to the more commonly studied flows of pure jets and plumes. That is, the direction of buoyancy does not fundamentally change the mechanisms driving turbulent mixing in NBJs in the Ri range explored here.

6. Conclusion

The present study has investigated the radial velocity, Reynolds stress and radial scalar flux profiles, h, j and p, for turbulent jets with arbitrary buoyancy. This includes the limiting cases of pure jets and plumes, as well as intermediary cases with both positive and negative buoyancies. All these flows have been documented to have Gaussian mean axial velocity and buoyancy/scalar profiles (Papanicolaou & List 1988; Panchapakesan & Lumley 1993; Wang & Law 2002; Milton-McGurk *et al.* 2021), and previous studies have used this information to derive expressions for the $\bar{u}$, $\overline{w'u'}$ and $\overline{u'b'}$ profiles in the limiting cases (Mih 1989; Agrawal & Prasad 2003). The present study builds on these approaches by generalising the expressions to arbitrary buoyancies, which are valid for PBJs and NBJs in addition to pure jets/plumes.

These analytical expressions were compared to profiles obtained from previous experimental and numerical studies in § 4. The profile predictions were found to be in agreement with the literature for all flows investigated at the local Richardson numbers presented. The expressions h, j and p may therefore be used to estimate $\bar{u}$, $\overline{w'u'}$ and $\overline{u'b'}$ in jets with arbitrary buoyancy, provided appropriate values of λ and δ_m are used. These depend on the local Ri being considered, with $\lambda = 1.0$ and $\delta_m = -0.20$ being suitable for $Ri > 0$ (PBJs and plumes), and $\lambda = 1.2$ and $\delta_m = -0.20$ for $Ri = 0$ (jets). NBJs, which have not been studied as extensively, require the empirical linear δ_m relation in (4.1) and $\lambda \simeq 1.46$, and show good agreement for $Ri \gtrsim -0.10$. These expressions may be useful for applications where directly measuring the profiles is challenging, such as in industrial applications or field settings, or simply for experimental or numerical researchers wishing to validate their data.

The h, j and p equations were used to derive expressions for turbulent momentum and thermal/mass diffusivity, and subsequently the turbulent Prandtl/Schmidt number. These were found to be constants in pure jets ($Ri = 0$) and plumes ($\lambda = 1$), with values in agreement with the previous literature. Under the present assumptions, constant Sc_T values occur in all jets that have $\lambda = 1$, which can reasonably describe PBJs and gives values consistent with existing literature (van Reeuwijk *et al.* 2016). The analytical result for an NBJ was presented against experimental data, which were found to be in agreement for $\eta \lesssim 2$, and were reasonably similar in magnitude to the neutral jet. This supports the argument that NBJs may be analysed with similar assumptions to the canonical cases of pure jets and plumes, and that the negative buoyancy does not fundamentally change the turbulent mixing in the Ri range investigated.

Declaration of interests. The authors report no conflict of interest.

Author ORCIDs.
L. Milton-McGurk https://orcid.org/0000-0002-4294-729X;
N. Williamson https://orcid.org/0000-0001-7246-8356;
S.W. Armfield https://orcid.org/0000-0002-8032-0017.

References

Agrawal, A. & Prasad, A.K. 2003 Integral solution for the mean flow profiles of turbulent jets, plumes, and wakes. *J. Fluids Engng* **125** (5), 813–822.

Carazzo, G., Kaminski, E. & Tait, S. 2006 The route to self-similarity in turbulent jets and plumes. *J. Fluid Mech.* **547**, 137–148.

Chen, C.J. & Rodi, W. 1980 Vertical turbulent buoyant jets: a review of experimental data. *NASA Sti/Recon Tech. Rep.* A **80**, 23073.

Craske, J., Salizzoni, P. & van Reeuwijk, M. 2017 The turbulent Prandtl number in a pure plume is 3/5. *J. Fluid Mech.* **822**, 774–790.

Darisse, A, Lemay, J. & Benaïssa, A. 2013 Investigation of passive scalar mixing in a turbulent free jet using simultaneous LDV and cold wire measurements. *Intl J. Heat Fluid Flow* **44**, 284–292.

Ezzamel, A., Salizzoni, P. & Hunt, G.R. 2015 Dynamical variability of axisymmetric buoyant plumes. *J. Fluid Mech.* **765**, 576–611.

Fischer, H.B., List, J.E., Koh, C.R., Imberger, J. & Brooks, N.H. 1979 *Mixing in Inland and Coastal Waters*. Academic.

Fox, D.G. 1970 Forced plume in a stratified fluid. *J. Geophys. Res.* **75** (33), 6818–6835.

Hunt, G.R. & Debugne, A.L.R. 2016 Forced fountains. *J. Fluid Mech.* **802**, 437–463.

Kaminski, E., Tait, S. & Carazzo, G. 2005 Turbulent entrainment in jets with arbitrary buoyancy. *J. Fluid Mech.* **526**, 361–376.

Mih, W.C. 1989 Equations for axisymmetric and twodimensional turbulent jets. *J. Hydraul. Engng* **115** (12), 1715–1719.

Milton-McGurk, L., Williamson, N., Armfield, S.W. & Kirkpatrick, M.P. 2020 Experimental investigation into turbulent negatively buoyant jets using combined PIV and PLIF measurements. *Intl J. Heat Fluid Flow* **82**, 108561.

Milton-McGurk, L., Williamson, N., Armfield, S.W. & Kirkpatrick, M.P. 2022 Characterising entrainment in fountains and negatively buoyant jets. *J. Fluid Mech.* **939**, A29.

Milton-McGurk, L., Williamson, N., Arfmfield, S.W., Kirkpatrick, M.P. & Talluru, K.M. 2021 Entrainment and structure of negatively buoyant jets. *J. Fluid Mech.* **911**, A21.

Morton, B.R. 1959 Forced plumes. *J. Fluid Mech.* **5** (1), 151–163.

Morton, B.R., Taylor, G.I. & Turner, J.S. 1956 Turbulent gravitational convection from maintained and instantaneous sources. *Proc. R. Soc. Lond.* A **234** (1196), 1–23.

Panchapakesan, N.R. & Lumley, J.L. 1993 Turbulence measurements in axisymmetric jets of air and helium. Part 1. Air jet. *J. Fluid Mech.* **246**, 197–223.

Papanicolaou, P.N. & List, E.J. 1988 Investigations of round vertical turbulent buoyant jets. *J. Fluid Mech.* **195**, 341–391.

Priestley, C.H.B. & Ball, F.K. 1955 Continuous convection from an isolated source of heat. *Q. J. R. Meteorol. Soc.* **81** (348), 144–157.

Rajaratnam, N. 1976 *Turbulent Jets*. Elsevier.

van Reeuwijk, M. & Craske, J. 2015 Energy-consistent entrainment relations for jets and plumes. *J. Fluid Mech.* **782**, 333–355.

van Reeuwijk, M., Salizzoni, P., Hunt, G.R. & Craske, J. 2016 Turbulent transport and entrainment in jets and plumes: a DNS study. *Phys. Rev. Fluids* **1** (7), 074301.

Shabbir, A. & George, W.K. 1994 Experiments on a round turbulent buoyant plume. *J. Fluid Mech.* **275**, 1–32.

Talluru, K.M., Armfield, S., Williamson, N., Kirkpatrick, M.P. & Milton-McGurk, L. 2021 Turbulence structure of neutral and negatively buoyant jets. *J. Fluid Mech.* **909**, A14.

Talluru, K.M., Williamson, N. & Armfield, S.W. 2022 Entrainment and dilution in a fountain top. *J. Fluid Mech.* **941**, A24.

Wang, H. & Law, A.W.-K. 2002 Second-order integral model for a round turbulent buoyant jet. *J. Fluid Mech.* **459**, 397–428.